Near-field spectroscopy of low-loss waveguide integrated microcavities

Benoit Cluzel, E. Picard, Thomas Charvolin, Emmanuel Hadji, Loïc Lalouat, Frédérique de Fornel, Christophe Sauvan, Philippe Lalanne

Near-field spectroscopy of low-loss waveguide integrated microcavities

B. Cluzel, E. Picard, T. Charvolin, E. Hadji, L. Lalouät et al.

Citation: Appl. Phys. Lett. **88**, 051112 (2006); doi: 10.1063/1.2170141
View online: http://dx.doi.org/10.1063/1.2170141
View Table of Contents: http://apl.aip.org/resource/1/APPLAB/v88/i5
Published by the American Institute of Physics.

Near-field spectroscopy of low-loss waveguide integrated microcavities

B. Cluzel, E. Picard, T. Charvolin, and E. Hadji[a)]
Laboratoire Silicium Nanoélectronique Photonique et Structure, Département de Recherche Fondamentale sur la Matière Condensée, Commissariat à l'Energie Atomique, 17 rue des Martyrs, F-38054 Grenoble Cedex, France

L. Lalouät and F. de Fornel
Laboratoire de Physique de l'Université de Bourgogne, Centre National de la Recherche Scientifique, 9 Avenue Alain Savary, Boîte Postale 47870, F-21078 Dijon Cedex, France

C. Sauvan and P. Lalanne
Laboratoire Charles Fabry de l'Institut d'Optique, Centre National de la Recherche Scientifique, F-91403 Orsay Cedex, France

(Received 4 October 2005; accepted 17 December 2005; published online 1 February 2006)

A scanning near-field spectroscopy method is used to observe loss reduction and *Q*-factor enhancement due to transverse-mode profile matching within photonic-crystal microcavities. Near-field measurements performed directly on cavity modes are compared with three-dimensional calculations and quantitative agreement is observed. © *2006 American Institute of Physics*.
[DOI: 10.1063/1.2170141]

Photonic band gap materials have attracted considerable interest in recent years due to their ability to control the propagation of photons inside semiconductors.[1] However, the methods most commonly used to date to examine their properties have been far-field techniques such as spectral analysis of out-of-plane radiated or transmitted light. Only a few recent studies have demonstrated the ability of scanning near-field optical microscopy (SNOM) techniques to *directly* examine aspects relating to the interaction between light and photonic crystals, such as coupling between the spontaneous emission of quantum dots and the optical modes of a hexagonal microcavity,[2] existence of ultraslow light propagation in a photonic crystal waveguide,[3] observation of Bloch harmonics,[4] Bloch mode parity change in photonic crystal waveguides,[5] or field confinement inside photonic crystal microcavities.[6,7]

In this study, we used a scanning near-field optical microscope to examine several photonic-crystal microcavities which were tuned to taper the slab mode inside the cavity into the photonic-crystal evanescent Bloch mode of the mirrors in order to reduce mode-profile mismatch at the cavity-mirror interfaces, and thus to enhance the *Q* factor of the cavity.[8]

The cavities consisted of Fabry-Pérot-like microcavities[9] created by omitting to drill one row of air holes inside a triangular-shaped photonic crystal etched in a silicon-on-insulator substrate. The period of the crystal was 375 nm, with a hole diameter of 190 nm. The whole structure was etched in a 8-μm-width multimode waveguide made of a 385-nm-thick crystalline silicon film on a 700-nm-thick buried oxide. Mode profile matching was obtained by tuning the position of the first rows of air holes surrounding the cavity (see Fig. 1), as has been proposed recently.[8,10] In addition, the tuning value, δ, was progressively varied using a 20 nm step from the so-called reference cavity (with periodic mirrors, $\delta=0$) to a value of 80 nm.

Structures were created using a two-step lithography process: the photonic crystal was defined, then the ridge waveguide was superimposed. Patterns on the resist were then transferred to the silicon film by using a chlorine-based

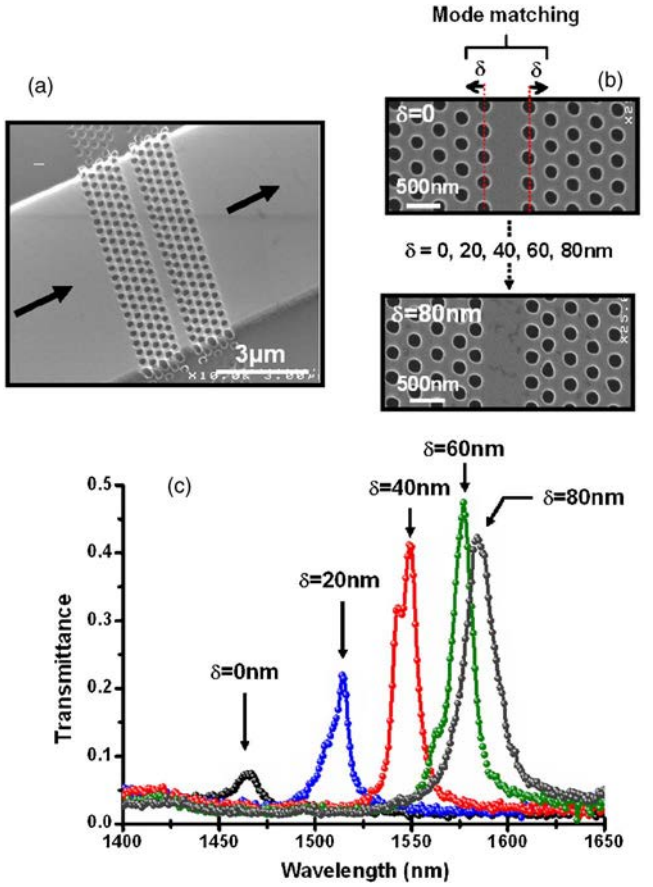

FIG. 1. (Color online) (a) SEM pictures of the investigated microcavities, (b) enlarged view of the cavities with row tuning of $\delta=0$ and 80 nm, and (c) experimental far-field transmittance spectra of the cavities. The corresponding values of δ are indicated. The transmittance values are absolute since the presented spectra are normalized by the transmission of an identical waveguide without cavity.

[a)]Electronic mail: emmanuel.hadji@cea.fr

inductively coupled plasma etching process with a 100-nm-thick silica hard mask. Scanning electron microscopy (SEM) pictures of the structures produced are shown in Figs. 1(a) and 1(b).

Each of the five cavities produced were then characterized using a waveguided spectroscopy technique.[5] The measured absolute transmittance spectra obtained for a TE polarization of light are shown in Fig. 1(c). The spectral range of the measurements shown is limited to the part of the photonic band gap (where transmittance is close to zero on the figure) which includes all cavity-mode resonances. These modes are indicated on the figure by the vertical arrows showing the corresponding δ values of the air-hole tuning.

Some of the observations are consistent with our understanding of the effect of hole tuning in photonic crystal microcavities.[8,11] As δ increases, the effective cavity length increases, and the resonance wavelength is redshifted.[11] More importantly, the mode profile mismatch at the mirror-cavity interfaces decreases with increasing values of δ. Thus radiation losses in the claddings are reduced and mirror performance increases. This is consistent with the evolution of peak transmittance at resonance, which increases from 8% to 50% for tuning values from 0 to 60 nm. For the 80 nm-tuned cavity, peak transmittance at resonance decreases again as a result of over-tuning with an increased mismatch.[8,11] However, a reduction in scattering losses at the cavity-mirror interfaces with hole tuning should result in higher Q-factor values.[11] This is not observed in the experimental data of Fig. 1, where Q factors are fairly constant ($\approx$150) for all cavities. In addition, this observation is inconsistent with Q-factor calculations, as will be discussed later.

To understand the reasons for these inconsistencies, near-field measurements were taken of the cavity modes. Considering the 20-nm-tuned microcavity, the SNOM probe, consisting of a chemically etched monomode optical fiber, was positioned 4 nm above the cavity by using shear-force feedback. Optical pictures were then recorded corresponding to different wavelengths inside the resonance peak observed in the transmittance measurement. The pictures obtained are shown in Fig. 2. On the figure, we have also superimposed the physical locations of the cavity holes, deduced from the topographical pictures recorded at the same time as the optical pictures. The light confined in the cavity is directly linked to the cavity-mode symmetry. In the two pictures, it is clear that, for each wavelength, we recorded the cavity modes corresponding respectively to the fundamental mode (TE_{00}) of the ridge waveguide (with a single maximum in the transverse direction of the waveguide) and the first-order mode (TE_{01}) (with a single node in the center of the waveguide). These measurements explain why no Q-factor enhancement was observed by air-hole tuning with far-field measurements in Fig. 1. The far-field transmission does not result from a single mode resonance but from the superposition of two transversal resonances.

To identify the contribution of each of these modes, we then moved the probe to two different positions (labeled *A* and *B* in the figures) above the cavity, each location corresponding to an intensity maximum of the TE_{00} and TE_{01} cavity modes, and used a tunable laser to perform a spectral analysis of the light collected by the probe at these locations. The recorded spectra are plotted on Fig. 2. The far-field transmittance spectrum of Fig. 1 is superimposed with a dashed line. We conclude that the far-field resonance measurement with an estimated Q factor equal to 120 results in fact from the overlap between the TE_{00} and the TE_{01} resonances with Q factors equal to 250 and 230, respectively.

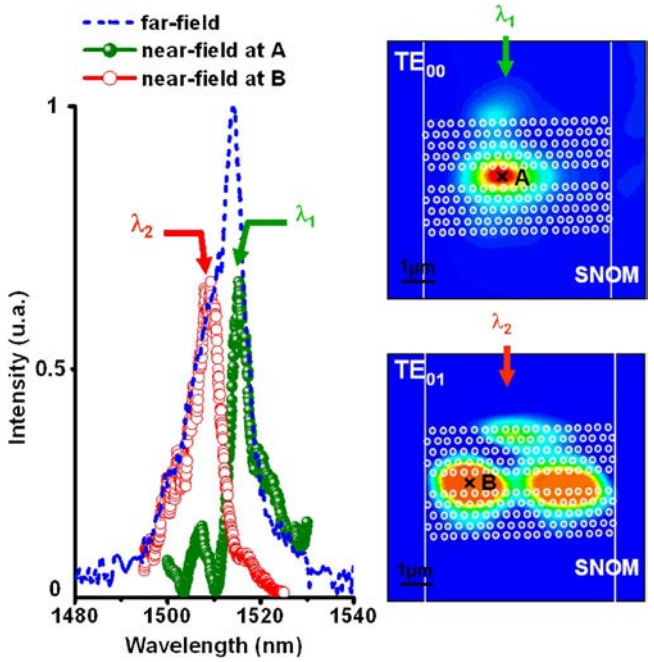

FIG. 2. (Color online) (Left) SNOM experimental spectra obtained for the cavity with 20 nm row tuning. The transmittance spectrum shown by a dashed-line is the same as in Fig. 1(c) and is obtained with far-field measurements. (Right) SNOM optical pictures recorded for two different wavelengths (λ_1 and λ_2) chosen inside the resonance peak obtained with far-field transmittance measurements. The locations of the cavity holes deduced from topographical pictures are superimposed on the SNOM pictures, and points *A* and *B* represent the exact locations of the probe when recording the corresponding near-field spectra.

We repeated the near-field spectra measurements for all the fabricated cavities, identifying the contribution of the TE_{00} and TE_{01} cavity modes for every case. Figure 3(a) shows the spectra corresponding solely to the resonance of the TE_{00} modes of each structure. All the spectra are normalized to the maximum intensity. We observe that the cavity Q factors increase from 120 for the reference cavity (δ=0) to 500 for a 60 nm tuning. Such behavior is now consistent with our understanding of the peak transmittance enhance-

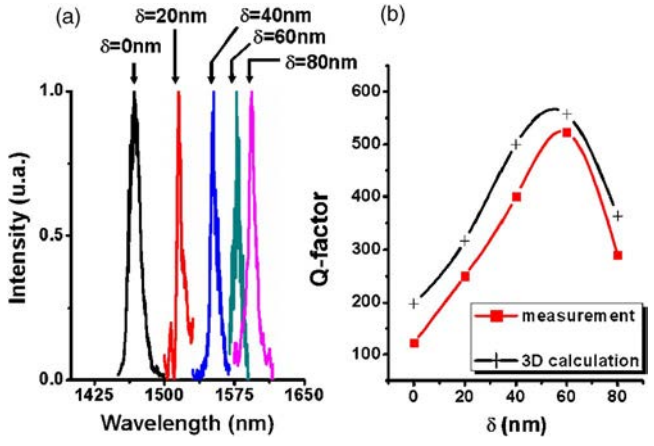

FIG. 3. (Color online) (a) Near-field spectra of the fundamental TE_{00} cavity-mode resonances obtained for δ=0, 20, 40, …80 nm. (b) Experimental and numerical Q-factor values as a function of tuning values.

ment obtained in Fig. 1 and observed earlier in far-field measurements.

Finally, we compared the near-field experimental measurements with computational data obtained with a three-dimensional (3D) vectorial modal method relying on Fourier expansion techniques.[12] The geometric parameters used for the computation were those actually measured on the samples. The refractive indices for the silicon slab and the SiO_2 substrate were assumed to be independent of the wavelength and were equal to 3.42 and 1.46, respectively. Experimental and numerical *Q*-factor values as a function of air hole tuning are plotted in Fig. 3(b). Quantitative agreement is obtained between near-field measurements and 3D calculations: the measured and computed *Q* factors exhibit identical variations with the hole-tuning parameter, with a maximum enhancement for $\delta = 60$ nm in both cases. The experimental values are slightly smaller, the weak difference being attributed to inevitable fabrication defects and to the Si substrate influence, neither of which are taken into account in the calculations.

To summarize, we fabricated waveguide integrated microcavities and performed near-field and far-field measurements for the resonance. It was shown that with proper transverse-mode profile tapering, the out-of-plane scattering at the cavity-mirror interfaces can be greatly reduced. As the inner rows of holes on the mirrors were displaced, we observed an increase in peak transmission at resonance from 8% to 50%, together with a five-fold *Q*-factor enhancement. In addition, by mapping the near-field distribution of the cavities, we observed the intricate contribution of the different guided modes supported by the structure. SNOM measurements enabled a precise interpretation of far-field observations, and revealed quantitative agreement between the experimental results and 3D calculations. This work demonstrates that near-field optical microscopy is a powerful tool in studying photonic band gap-material devices.

This work has been supported by the French ministry in charge of research with the ACI NR 063 *Chabip*. B.C. is also grateful to the Conseil Régional de Bourgogne for financial support, while C.S. received financial assistance from the Délégation Générale pour l'Armement.

[1] J. D. Joannopoulos, R. D. Meade, and J. N. Winn, *Photonic Crystals: Molding the Flow of Light* (Princeton University Press, Princeton, NJ, 1995).
[2] N. Louvion, D. Gérard, J. Mouette, F. de Fornel, C. Seassal, X. Letartre, A. Rahmani, and S. Callard, Phys. Rev. Lett. **94**, 113907 (2005).
[3] H. Gersen, T. J. Karle, R. J. P. Engelen, W. Bogaerts, J. P. Korterik, N. F. Van Hulst, T. F. Krauss, and L. Kuipers, Phys. Rev. Lett. **94**, 73903 (2005).
[4] H. Gersen, T. J. Karle, R. J. P. Engelen, W. Bogaerts, J. P. Korterik, N. F. Van Hulst, T. F. Krauss, and L. Kuipers, Phys. Rev. Lett. **94**, 123901 (2005).
[5] B. Cluzel, D. Gérard, E. Picard, T. Charvolin, V Calvo, E. Hadji, and F. de Fornel, Appl. Phys. Lett. **85**, 2682 (2004).
[6] P. Kramper, M. Kafesaki, C. M. Soukoulis, A. Birner, F. Müller, U. Gösele, R. B. Wehrspohn, J. Mlynek, and V. Sandoghdar, Opt. Lett. **29**, 174 (2004).
[7] B. Cluzel, D. Gérard, E. Picard, T. Charvolin, F. de Fornel, and E. Hadji, J. Appl. Phys. (to be published).
[8] C. Sauvan, G. Lecamp, P. Lalanne, and J. P. Hugonin, Opt. Express **13**, 245 (2005).
[9] M. Zelsmann, E. Picard, T. Charvolin, E. Hadji, B. Dal'zotto, M. E. Nier, C. Seassal, P. Rojo-Romeo, and X. Letartre, Appl. Phys. Lett. **81**, 2340 (2002).
[10] Y. Akahane, T. Asano, B. S. Song, and S. Noda, Nature **245**, 944 (2003).
[11] C. Sauvan, P. Lalanne, and J. P. Hugonin, Phys. Rev. B **71**, 165118 (2005).
[12] E. Silberstein, P. Lalanne, J. P. Hugonin, and Q. Cao, J. Opt. Soc. Am. A **18**, 2865 (2001).